Title

A Capacitively-Isolated Dual Extended LC-tank Hybrid Switched-Capacitor Converter

Authors

Jackson, Amanda
Ellis, Nathan M
Pilawa-Podgurski, Robert CN

Publication Date

2022-03-24

DOI

10.1109/apec43599.2022.9773640

A Capacitively-Isolated Dual Extended LC-tank Hybrid Switched-Capacitor Converter

Amanda Jackson, Nathan M. Ellis, Robert C.N. Pilawa-Podgurski
Dept. of Electrical Engineering and Computer Sciences
University of California, Berkeley, U.S.A.
Email: {amandajackson, nathanmilesellis, pilawa} @berkeley.edu

***Abstract*—This work introduces a resonant Dickson-type converter topology whose flying capacitors provide dielectric isolation between input and output terminals. For even conversion ratios, it achieves complete soft-charging of all of its flying capacitors with a convenient 50% duty cycle. Additionally, switch count is reduced relative to prior work and no distributed bypass capacitor column is required. Moreover, this topology actively drives both of its inductors without the requirement for mutual coupling between magnetic elements. A discrete 4:1 hardware prototype designed for 48 V up to rectified US mains applications is demonstrated and achieves a high power density of 2,010 W/in^3 with a 140 V input voltage and 941 kHz switching frequency.**

***Index Terms*—DC-DC power conversion, isolated, hybrid switched-capacitor.**

I. Introduction

In recent years, hybrid switched-capacitor (hybrid-SC) converters have shown promising results, achieving very high power densities at moderate to large conversion ratios [1]–[6]. These converters take advantage of the high energy density of capacitors while utilizing minimal inductance to achieve soft-charging [7], [8] and mitigate the slow-switching limit (SSL) that has long limited the feasibility of purely capacitor-based converters [9]. However, most work in this space has focused on non-isolated topologies, whereas many applications require isolation.

High power density can be challenging to achieve with conventional isolated converters that typically employ large and heavy transformers to achieve galvanic isolation. Thus, with the continual demand for smaller and lighter power electronics, hybrid-SC solutions that introduce a dielectric barrier between input and output have gained attention as possible cost-effective isolation alternatives to purely magnetic-based approaches [10]–[12].

Prior work has demonstrated the viability of converters with capacitive isolation (e.g. Fig. 1a and 1b), although these prototypes do not emphasize the power densities achievable with modern hybrid-SC design, with Fig. 1a additionally being incapable of complete soft-charging. Conversely, the non-isolated topology depicted in Fig. 1c [5] has recently demonstrated very high power densities with a reduced part count for a given conversion ratio. This is due to a reduction in the number of required switches and elimination of the large (theoretically infinite in size) bypass capacitor column that the topologies in Fig. 1a and 1b rely on.

As such, the topology proposed in this work (Fig. 1d) is a capacitively-isolated variant of the Dickson-type topology described in [5]. It maintains favorable features, such as: complete soft-charging with two-phase operation and a 50% duty cycle; the lack of a bypass capacitor column requirement; and load-independent switch stress. Additionally, in contrast to Fig. 1b, the proposed converter actively drives both of its inductors 180° out of phase and therefore does not require magnetic coupling to drive a full bridge output stage.

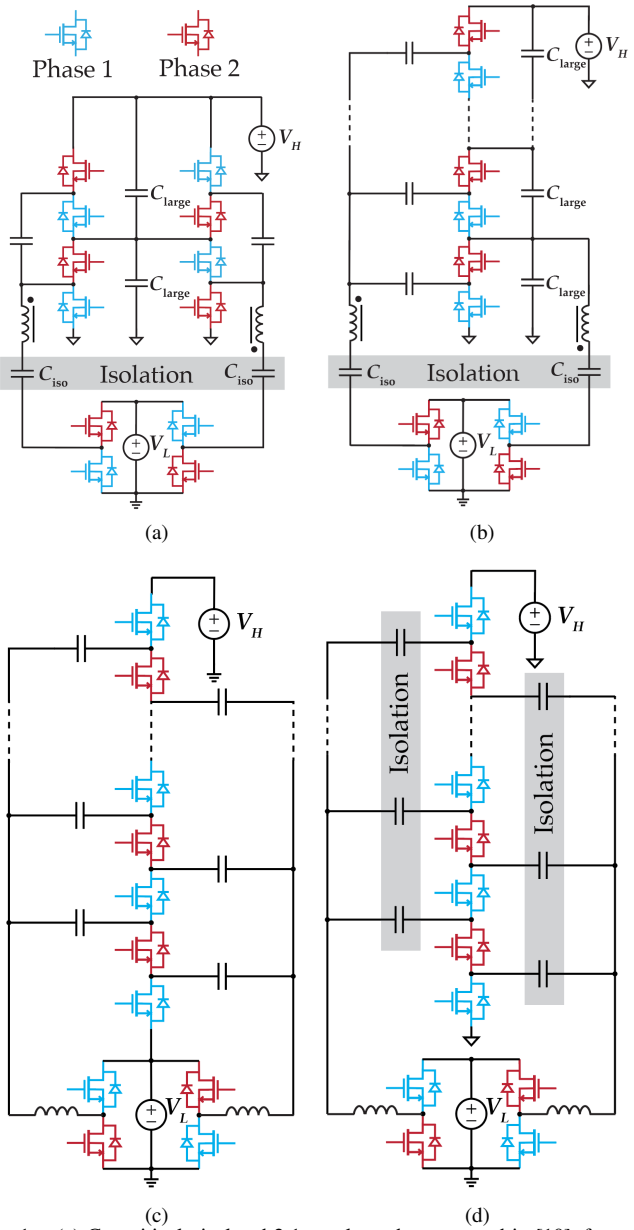

Fig. 1. (a) Capacitively isolated 2:1 topology demonstrated in [10], featuring mutually coupled inductors and two dedicated isolation capacitors. (b) More recent single-ended N:1 isolated topology [12]. Since the right-side inductor is tied to a static DC bias, full mutual coupling between both inductors is required in order to drive the low-side full-bridge. (c) The Dual Extended LC-tank converter recently demonstrated in [5]. This non-isolated topology does not require mutual coupling between its two inductors. (d) Proposed topology of this work, similar to (c) but with two separate reference voltages, allowing flying capacitors to act as an isolation barrier.

Furthermore, we note that lower-voltage switches typically exhibit higher figures of merit [13], [14]. As such, stacked or ladder-type topologies containing switches with lower voltage ratings relative to the high voltage bus can be expected to offer improved performance relative to conventional converters such as the dual-active bridge, whose switches must tolerate the full input voltage.

Finally, although this work focuses on resonant two-phase fixed-conversion-ratio operation, the proposed topology is amenable to complete zero voltage switching (ZVS) and voltage regulation through phase shifted operation, similar to that demonstrated in [12].

II. Theory of Operation

To determine the converter's periodic steady-state resonant behavior, charge-flow analysis [9] is employed to deduce the relative charge flow through the converter: the normalized high-side charge quantity q is used to annotate Fig. 3. From this, the conversion ratio can be determined: for the level count demonstrated in this work, an average of four units of charge exit the converter for every single unit of charge that enters the converter, so $I_{\mathrm{L}} = 4 \times I_{\mathrm{H}}$, with I_{L} and I_{H} indicating low-side and high-side current respectively. In this ideal analysis, input power and output power are equal, which implies $V_{\mathrm{H}} = 4V_{\mathrm{L}}$, or a 4:1 conversion ratio.

In addition, charge-flow analysis informs the voltage ripple seen across each flying capacitor. In this design, all flying capacitors have equal value C, and each capacitor experiences charge flow q during a single phase. Defining f_{sw} as the converter switching frequency, the AC flying capacitor voltage ripple Δ, annotated in Fig. 3, is calculated as

$$2\Delta \ \ (\text{Volts}) = \frac{q}{C} = \frac{I_{\mathrm{H}}}{f_{\mathrm{sw}} C} \tag{1}$$

Whether a capacitor increases or decreases by 2Δ during a phase depends on the direction of charge flow within a given phase and is signified by $\pm$ and $\mp$ notation. Applying Kirchoff's voltage law (KVL) to Fig. 3, either at the start or end of both phases, two equations are obtained that are independent of AC ripple Δ.

$$-V_1 - V_2 + V_3 + V_4 = V_H \tag{2}$$

$$V_1 - V_2 - V_3 + V_4 = 0 \tag{3}$$

where V_i is the DC voltage across the i^{th} capacitor. Furthermore, by assuming resonant zero-current switching between phases, it can be deduced that in the middle of each phase, each flying capacitor C_i has voltage V_i, with no Δ component, and both inductors incur 0 V across each of them. As such, two additional equations are obtained during phase 1.

$$V_1 = V_{\mathrm{ISO}} \tag{4}$$

$$V_{\mathrm{L}} + V_4 = V_{\mathrm{H}} + V_{\mathrm{ISO}} \tag{5}$$

where V_{ISO} is the voltage difference between the isolated reference node connected to the source of Q_1 and ground. Solving (2)-(5) yields

$$V_1 = V_{\mathrm{ISO}} \tag{6}$$

$$V_2 = V_{\mathrm{L}} + V_{\mathrm{ISO}} = \frac{V_{\mathrm{H}}}{4} + V_{\mathrm{ISO}} \tag{7}$$

$$V_3 = 2V_{\mathrm{L}} + V_{\mathrm{ISO}} = \frac{V_{\mathrm{H}}}{2} + V_{\mathrm{ISO}} \tag{8}$$

$$V_4 = 3V_{\mathrm{L}} + V_{\mathrm{ISO}} = \frac{3V_{\mathrm{H}}}{4} + V_{\mathrm{ISO}} \tag{9}$$

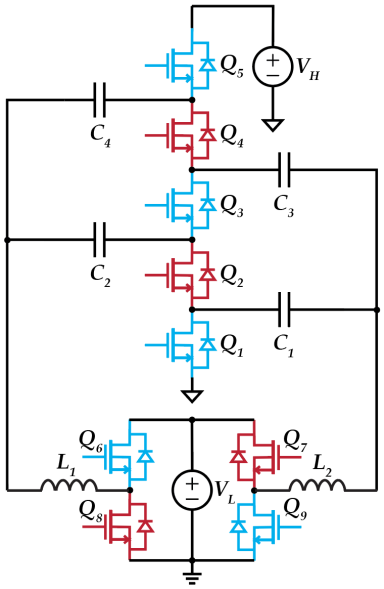

Fig. 2. Example 4:1 schematic of the proposed capacitively-isolated extended LC-tank converter.

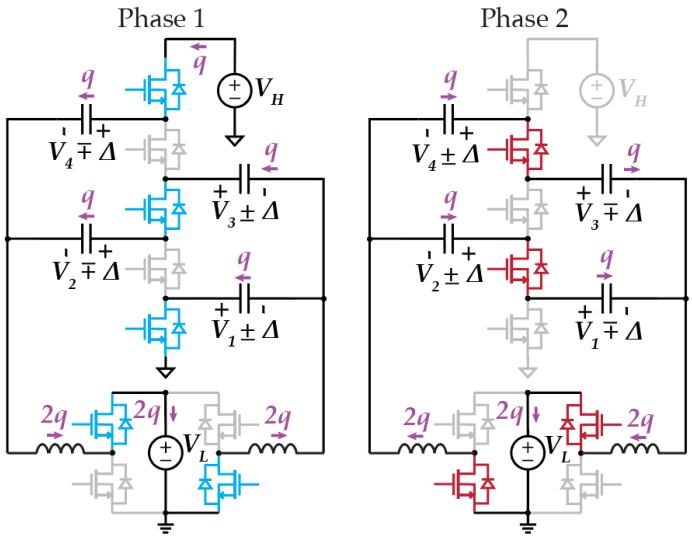

Fig. 3. Converter schematic in each phase, annotated with charge-flow analysis and capacitor voltage ripple. $\pm$ indicates a voltage ripple that transitions from a more positive voltage at the beginning of the phase to a more negative voltage at the end of the phase, while $\mp$ denotes the reverse.

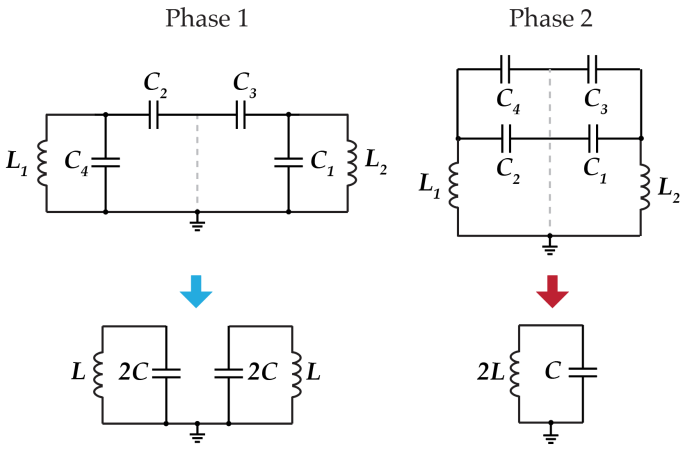

Fig. 4. Derived AC models of the proposed 4:1 converter in each phase. Since all capacitors are set equal in size, both phases can be simplified into LC resonant tanks with identical resonant frequencies.

The existence of a solution to (2)-(5) implies that all flying capacitors undergo complete soft-charging, with KVL being satisfied at all times [15]. This result is verified in hardware in Section III. Additionally, using similar KVL analysis to define the blocking voltages of inactive switches during both phases, voltage stress on all switches is determined to be a function of input and output voltages only and independent of load, reducing the switches' voltage rating requirements.

To determine the converter's natural resonant switching frequency f_{sw}, an equivalent AC model for each phase is created, as shown in Fig. 4. Setting both inductances equal to L, all capacitors equal to C, and noting that the nodes between two series capacitors acts as a virtual ground, it is apparent that in Phase 1 there are two identical equivalent LC tanks, each with inductance L and capacitance $2C$. Similarly, in Phase 2, there is one LC tank with equivalent inductance $2L$ and capacitance C. Therefore, the resonant frequency in each phase is calculated as follows:

$$f_{\text{sw},1} = \frac{1}{2\pi\sqrt{L \cdot 2C}} \tag{10}$$

$$f_{\text{sw},2} = \frac{1}{2\pi\sqrt{2L \cdot C}} \tag{11}$$

Since these two resonant frequencies are equal, the converter is operated at a convenient 50% duty cycle, significantly simplifying control of the switches.

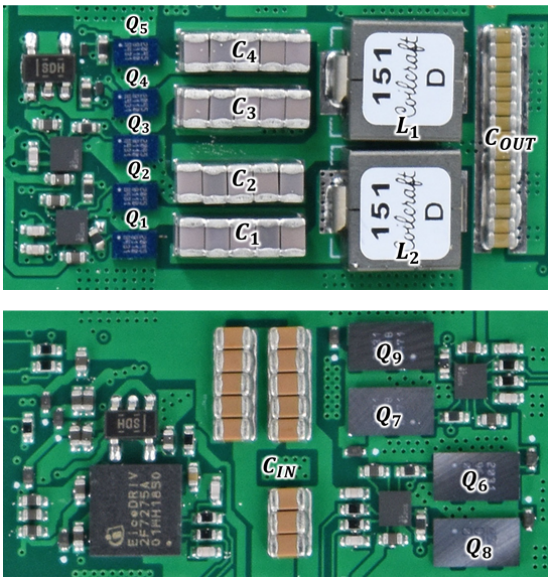

Fig. 5. Photograph of the constructed hardware prototype with dimensions 28.6 mm × 13.4 mm × 7.65 mm. Switches Q_{1-5}, flying capacitors C_{1-4}, inductors L_1 and L_2, and output capacitors are visible on the top side of the PCB (upper figure), while switches Q_{6-9} and input capacitors are visible on the PCB reverse (lower figure).

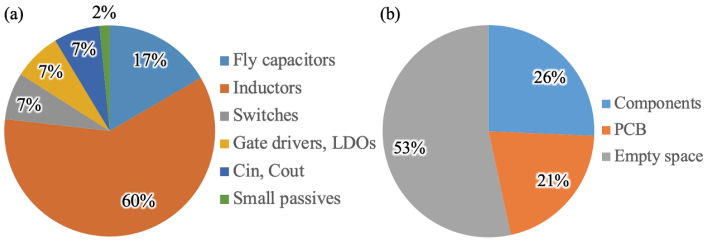

Fig. 6. Component volume breakdown (a), and total volume breakdown (b), demonstrating limits on volume imposed by inductor size and height.

III. Hardware Prototype

For ease of implementation and real-world applicability, the hardware prototype is a 4:1 variant, catering to 48 V-to-12 V conversion, but is also rated for a maximum 170 V input, emulating rectified US AC mains. With the converter operating at its resonant frequency of nearly 1 MHz, gallium nitride (GaN) devices were chosen due to their fast switching speed and reduced losses. To maintain a constant resonant frequency, flying capacitors with stable Class 1 C0G dielectrics were chosen and rated at 250 V to provide an isolation barrier that can be directly compared with [12]. Note that capacitors with a Y-rating may be required for use in practical consumer applications and may result in a significant capacitor volume increase. The selected inductors have a stable ferrite core material to ensure a relatively constant resonant frequency and are shielded to prevent any undesired magnetic coupling.

In the experimental setup, the converter's input was driven by a TDK-Lambda GEN300-5 300 V, 5 A power supply, and the output was connected to a BK Precision 8614 120 V, 240 A, 1.5 kW electronic load. On-board remote input and output voltage sensing headers were connected, respectively, to a Yokogawa WT310 power analyzer and the e-load to enable accurate measurement of input and output power. To ensure intended converter operation without control complications, open loop clock signals were provided by a Tektronix HFS 9003 clock generator controlled by MATLAB over GPIB. The converter was air-cooled with a standard 12 V computer fan. All waveforms were collected with a 200 MHz Keysight oscilloscope.

Fig. 5 depicts an annotated photograph of the constructed prototype, with component and total volume breakdown presented in Fig. 6. Figures 7 and 8 demonstrate operation, with Fig. 7 illustrating smooth sinusoidal flying capacitor voltages, signifying complete soft-charging and SSL mitigation.

At an input voltage of 120 V and switching frequency of 941 kHz, the converter prototype demonstrated a peak efficiency of 94.1% (including gate drive loss), shown in Fig. 9. With a peak power output of 359.6 W at an input voltage of 140 V and a best-fit box volume of 2,931 mm^3 (Fig. 6), the peak power density measured with hardware was 122.7 kW/L, or 2,010 W/in^3.

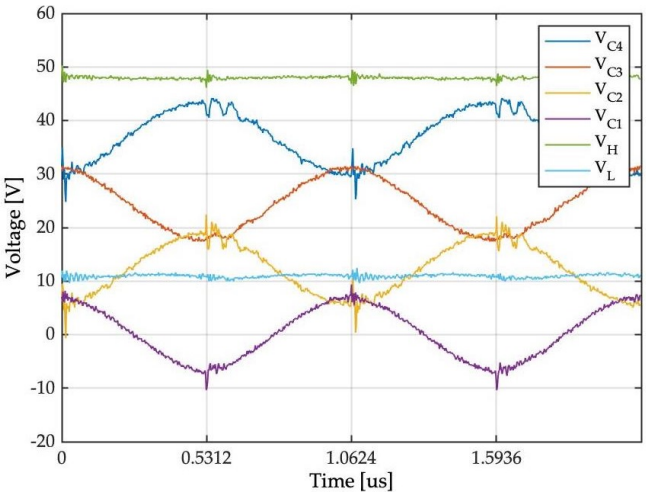

Fig. 7. Measured voltage waveforms of a 4:1 resonant prototype switching at 941 kHz and with an input voltage $V_H = 48$ V. Smooth sinusoidal voltage ripple across flying capacitors C_{1-4} illustrates complete soft-charging with no SSL losses.

TABLE I
COMPONENT DETAILS

Component	Part Number	Details
Q_{1-5}	EPC2045	5.6 mΩ, 100 V, 16 A
Q_{6-9}	EPC2031	2 mΩ, 60 V, 48 A
L_{1-2}	SLC7649S-151KLC	150 nH
C_{fly}	C2012C0G2E103K125AA	10x 10 nF 250 V C0G 0805
C_{in}	C2012X7T2E104M125AE	13x 0.1 uF 250 V X7T 0805
C_{out}	CL10B104KB8NNNL	15x 0.1 uF 50V X7R 0603
Gate Driver (Q_{4-5})	2EDF7275KXUMA1	4 A / 8 A, 460 V
Gate Driver ($Q_{1-3,6-9}$)	LMG1205YFXR	1.2 A / 5 A, 100 V
Bootstrap Diodes	CMAD4448	120 V, 250 mA

TABLE II
COMPARISON WITH PRIOR ART

	[1] APEC 2018	[16] APEC 2015	[5] APEC 2021	[12] COMPEL 2018	**This Work**
Topology	4:1 Cascaded Doubler	1:4 Dickson	1:5 Dickson	4:1 Res-Stack	**4:1 Dickson**
Isolation	No	No	No	Yes	**Yes**
Switching Scheme	2-Phase (50% Duty)	Split-Phase (Complex)	2-Phase (50% Duty)	2-Phase (50% Duty)	**2-Phase (50% Duty)**
Switch Type	MOSFET	GaN	GaN + Diodes	GaN	**GaN**
# of Inductors	2	1	2	2 (Coupled)	**2**
C_{fly} Ripple Limiter	Switch	Switch	Switch	Dielectric	**Dielectric**
f_{sw}	100 kHz	1.2 MHz	1.2 MHz	620 kHz	**941 kHz**
% Peak Eff.	98.9%	92%	94%	92.8%	**94.1%**
$P_{\text{out,max}}$	600 W	263 W	129 W	60 W	**360 W**
V_{L} @ $P_{\text{out,max}}$	15 V	33 V	19.8 V	12 V	**34 V**
V_{H} @ $P_{\text{out,max}}$	60 V	117 V	82.2 V	52 V	**140 V**
Power Density (Best-Fit Cuboid)	133 kW/L (2,180 W/in^3)	61.7 kW/L (1,011 W/in^3)	311 kW/L (5,096 W/in^3)	17.2 kW/L (283 W/in^3)	**122.7 kW/L (2,010 W/in^3)**

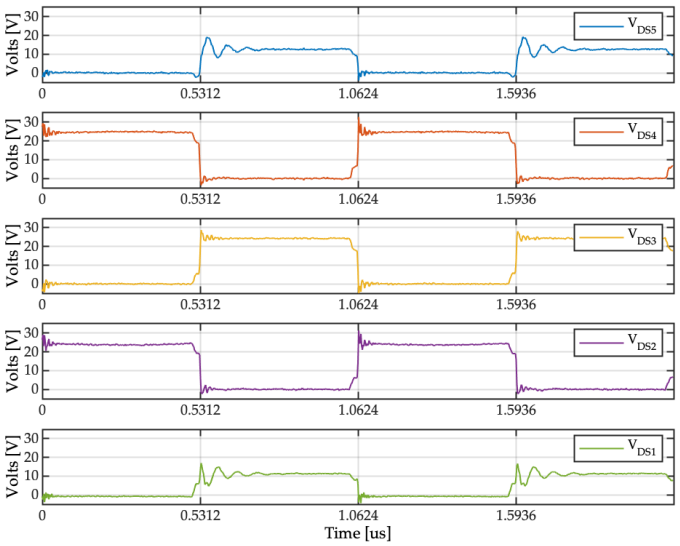

Fig. 8. Measured switch voltages with $V_{\text{H}} = 48$ V. All switches are seen to have a blocking voltage that is virtually flat, with no load-dependent voltage ripple imposed. In addition, partial zero-voltage switching (ZVS) is observed on the falling edges, with a noticeable decrease in voltage before switching occurs. Complete ZVS will be fully realized in future work.

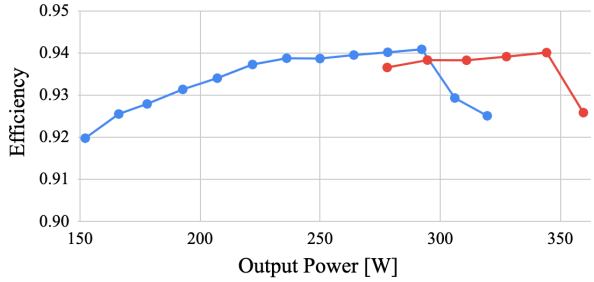

Fig. 9. Measured converter efficiency, including gate drive loss, across a range of loads with $V_{\text{H}} = 120$ V (blue) and $V_{\text{H}} = 140$ V (red).

IV. CONCLUSION AND FUTURE WORK

This work presents a Dickson-type topology exhibiting capacitive isolation and a reduced component count relative to similar hybrid switched-capacitor approaches of the same network order. Isolation is provided by the dielectrics of flying capacitors contained within a pair of extended LC-tanks. This topology's capability for two-phase resonant operation with a 50% duty cycle and complete soft-charging was derived and validated in hardware with a 4:1 prototype. Furthermore, while both inductors may benefit from mutual coupling due to their 180° shift in conduction, we note that this is not a requirement for correct operation, and separate discrete inductors are used in this work. Moreover, this topology is expected to be capable of complete ZVS and voltage regulation with adjustments made to its clocking scheme. As a result, improvements in efficiency and versatility are expected in future revisions. As is, the hardware prototype achieved a peak power of 359.6 W at 140 V input, corresponding to a high power density of 2,010 W/in^3 that is competitive with both recent isolated and non-isolated work (Table II).

REFERENCES

[1] Z. Ye, Y. Lei, and R. C. Pilawa-Podgurski, "A resonant switched capacitor based 4-to-1 bus converter achieving 2180 W/in^3 power density and 98.9 % peak efficiency," in *2018 IEEE Applied Power Electronics Conference and Exposition (APEC)*. IEEE, 2018, pp. 121–126.

[2] R. Das, G.-S. Seo, and H.-P. Le, "A 120 V - to - 1.8 V 91.5 %-Efficient 36-W Dual-Inductor Hybrid Converter with Natural Soft-charging Operations for Direct Extreme Conversion Ratios," in *2018 IEEE Energy Conversion Congress and Exposition (ECCE)*. IEEE, 2018, pp. 1266–1271.

[3] G.-S. Seo, R. Das, and H.-P. Le, "A 95 %-efficient 48 V - to - 1 V/10 A VRM hybrid converter using interleaved dual inductors," in *2018 IEEE Energy Conversion Congress and Exposition (ECCE)*. IEEE, 2018, pp. 3825–3830.

[4] N. Ellis and R. Amirtharajah, "A Resonant 1: 5 Cockcroft-Walton Converter Utilizing GaN FET Switches with N-Phase and Split-Phase Clocking," in *2020 IEEE Applied Power Electronics Conference and Exposition (APEC)*. IEEE, 2020, pp. 19–25.

[5] N. M. Ellis and R. Amirtharajah, "A resonant dual extended lc-tank dickson converter with 50% two-phase operation at odd conversion ratios," in *2021 IEEE Applied Power Electronics Conference and Exposition (APEC)*, 2021, pp. 1282–1287.

[6] T. Ge, Z. Ye, R. A. Abramson, and R. C. Pilawa-Podgurski, "A 48-to-12 v cascaded resonant switched-capacitor converter achieving 4068 w/in 3 power density and 99.0% peak efficiency," in *2021 IEEE Applied Power Electronics Conference and Exposition (APEC)*. IEEE, 2021, pp. 1335–1342.

[7] R. C. Pilawa-Podgurski, D. M. Giuliano, and D. J. Perreault, "Merged two-stage power converterarchitecture with softcharging switched-capacitor energy transfer," in *2008 IEEE Power Electronics Specialists Conference*. IEEE, 2008, pp. 4008–4015.

[8] Y. Lei and R. C. N. Pilawa-Podgurski, "A general method for analyzing resonant and soft-charging operation of switched-capacitor converters," *IEEE Transactions on Power Electronics*, vol. 30, no. 10, pp. 5650–5664, 2015.

[9] M. D. Seeman and S. R. Sanders, "Analysis and optimization of switched-capacitor dc–dc converters," *IEEE Transactions on Power Electronics*, vol. 23, no. 2, pp. 841–851, 2008.

[10] M. Kline, I. Izyumin, B. Boser, and S. Sanders, "A transformerless galvanically isolated switched capacitor led driver," in *2012 Twenty-Seventh Annual IEEE Applied Power Electronics Conference and Exposition (APEC)*, 2012, pp. 2357–2360.

[11] C. Le, M. Kline, D. L. Gerber, S. R. Sanders, and P. R. Kinget, "A stackable switched-capacitor dc/dc converter ic for led drivers with 90% efficiency," in *Proceedings of the IEEE 2013 Custom Integrated Circuits Conference*. IEEE, 2013, pp. 1–4.

[12] Y. Li, L. Gu, A. Hariya, Y. Ishizuka, J. Rivas-Davila, and S. Sanders, "A wide input range isolated stacked resonant switched-capacitor dc-dc converter for high conversion ratios," in *2018 IEEE 19th Workshop on Control and Modeling for Power Electronics (COMPEL)*, 2018, pp. 1–7.

[13] R. A. Abramson, S. J. Gunter, D. M. Otten, K. K. Afridi, and D. J. Perreault, "Design and evaluation of a reconfigurable stacked active bridge dc/dc converter for efficient wide load-range operation," in *2017 IEEE Applied Power Electronics Conference and Exposition (APEC)*, 2017, pp. 3391–3401.

[14] A. Lidow, M. De Rooij, J. Strydom, D. Reusch, and J. Glaser, *GaN transistors for efficient power conversion*. John Wiley & Sons, 2019.

[15] Y. Lei and R. C. Pilawa-Podgurski, "Analysis of switched-capacitor DC-DC converters in soft-charging operation," in *2013 IEEE 14th Workshop on Control and Modeling for Power Electronics (COMPEL)*. IEEE, 2013, pp. 1–7.

[16] B. B. Macy, Y. Lei, and R. C. Pilawa-Podgurski, "A 1.2 MHz, 25 V to 100 V GaN-based resonant Dickson switched-capacitor converter with 1011 W/in^3 (61.7 kW/L) power density," in *2015 IEEE Applied Power Electronics Conference and Exposition (APEC)*. IEEE, 2015, pp. 1472–1478.